ASEN 6037 - Final Project

Simulation of a hypersonic 2D compression corner

Kal Monroe

January 10, 2023

1 Introduction and Motivation

With regard to the design of hypersonic vehicles, important design considerations center around the design of control surfaces such as body flaps and elevons. However at hypersonic speeds, deflection of these surfaces is likely to result in the formation of an oblique shock, the interactions of which with the boundary layer create a region of flow separation and recirculation. These interactions can cause changes in vehicle dynamics as well as regions of severely high heating on the body - resulting in vehicle critical constraints on it's trajectory.

To better understand this interaction region, Simeonides and Haase (1995) performed joint hypersonic simulations and experimental studies on a 15° compression corner. A full Navier-Stokes solver using the algebraic Cebeci-Smith turbulence model as well as a state of the art hypersonic wind tunnel with semi-empirical corrections were used. In both computational and experimental results a region of highly separated flow was observed near the corner. Coefficients of heating and pressure are calculated along the wall of the corner and are shown to be in moderate agreement compared to experimental results.

The purpose of the current study is to repeat the results of Simeonides and Haase (1995) with the addition of several different turbulence models, namely, Baldwin-Lomax (BL), Menter Shear Stress Transport (SST), and the Spalart-Allmaras (SA) models. First, simulation geometry, boundary conditions, and grid characteristics are discussed. A laminar case is used to serve as an initial condition for the three turbulence models. Results for the BL, SST, and SA cases are then presented, discussed, and compared to the results of Simeonides and Haase (1995).

2 Simulation Setup

2.1 Simulation Geometry

To mimic the design of a control surface and study the interaction between recirculation zones and shockwaves, a 15° compression corner was selected. This geometry is comprised of a flat plate and an inclined ramp, both of length 0.2 m, as seen in Figure 1.

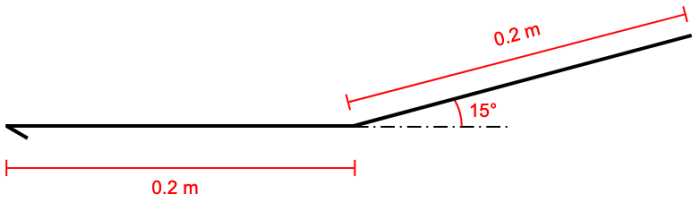

Figure 1: Compression corner geometry of test case 3 from Simeonides and Haase (1995).

Simeonides and Haase (1995) performed studies on several different ramp geometries, varying parameters such as the ramp hinge location, resulting in three test cases. To limit the scope of the current project the third test case was selected.

2.2 Computational Setup

A computational mesh of $[n_x,\ n_y] = [604,\ 250]$ was created to discretize the chosen geometry. Grid stretching was employed to ensure high resolution near the boundary layer as well as the expected recirculation zone near the corner. A wall normal spacing of 5×10^{-6} m was chosen to ensure a cell Reynolds number of O(1). A viscous wall condition was chosen to define the ramp geometry. The final mesh can be seen in Figure 2.

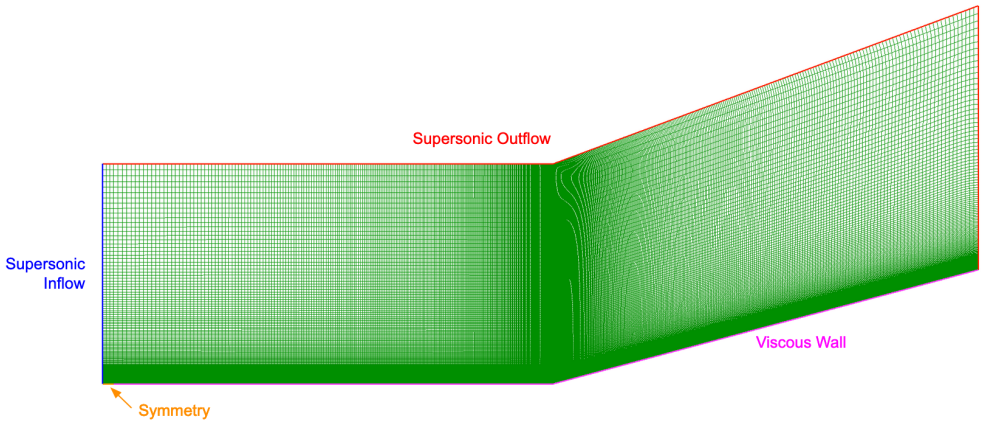

Figure 2: Computational domain for the 15° compression corner.

Freestream conditions were chosen to mimic the computational and experimental setup of Simeonides and Haase (1995). These can be summarized in Table 1.

Property	Test Case 3
Freestream Mach	14.1
Freestream temperature [K]	58.5
Unit Reynolds Number [1/m]	13×10^6
Isothermal wall temperature [K]	290
Working Fluid	N_2

Table 1: Test case 3 parameters

All simulations were run using LeMANS. LeMANS is a parallel, three-dimensional finite-volume CFD code that solves the Navier-Stokes and chemical reaction equations on unstructured grids with second-order spatial accuracy. A modified Steger-Warming flux vector splitting scheme is used to discretize the inviscid fluxes across cell faces. Viscous terms are computed using cell-centered and nodal values. Mixture transport properties are calculated using Wilke's semi-empirical mixing rule and species thermal conductivities are calculated using Eucken's relation. In accordance to the simulations of Simeonides and Haase (1995), this report does not consider chemistry.

3 Results from Simeonides and Haase (1995)

For test case 3, Simeonides and Haase (1995) created plots of pressure coefficient c_p and heating c_h (figures 3 and 5) along the surface. These were calculated according to the following formulas.

$$c_p = \frac{p - p_\infty}{\frac{1}{2}\rho_\infty v_\infty^2}$$

$$c_h = \frac{\dot{q}}{\rho_\infty v_\infty c_{p_\infty}(T_0 - T_w)}$$

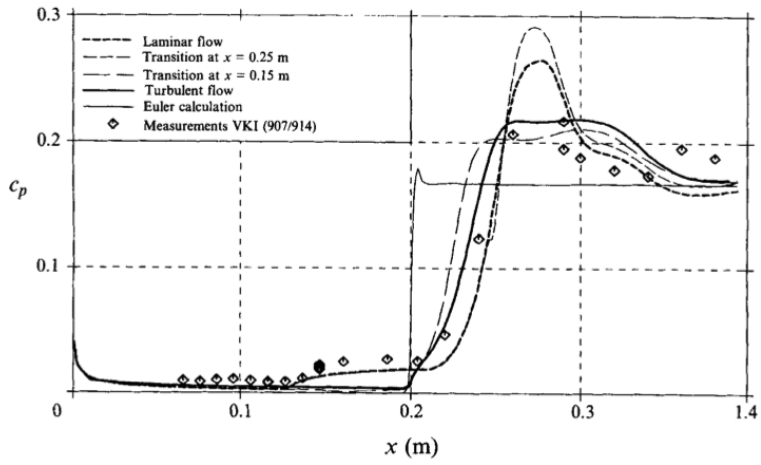

Figure 3: Pressure coefficient c_p along the wall for test case 3 by Simeonides and Haase (1995).

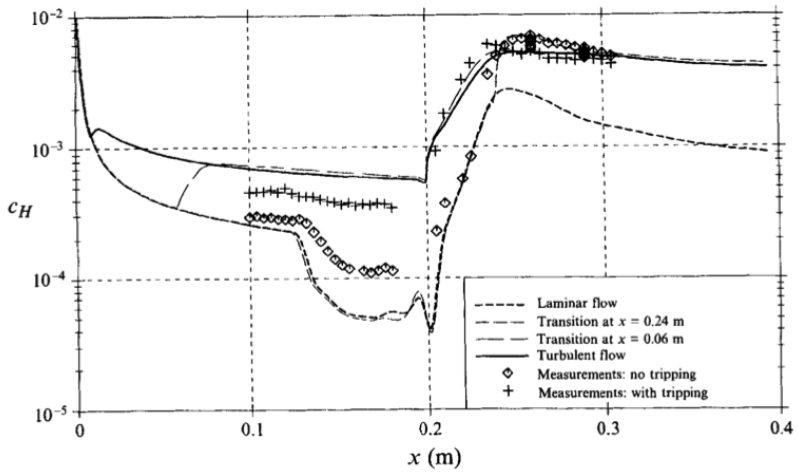

Figure 4: Heating coefficient c_h along the wall for test case 3 by Simeonides and Haase (1995).

For the laminar case, it is noted that c_p peaks after the corner near $x = 0.275$ m. In addition, values of c_h are seen to sharply decline near the start of the recirculation zone at $x = 0.14$ m. Interestingly, these phenomenon are not seen in the turbulent simulations, though the turbulent case is seen to have much higher values of c_h over the entire geometry. This is expected as turbulent boundary layers are known to increase mixing and aid in the transport of high enthalpy flow toward the wall. Overall, however, experimental results are seen to be in rough agreement near the compression corner and tend to follow the turbulent case.

Finally for a visual reference, Simeonides and Haase (1995) created Schlieren photographs, one of which is seen below. Note that the recirculation zone is between the corner and the oblique shock directly above it. The flow then reattaches along the inclined ramp and another oblique shock is formed.

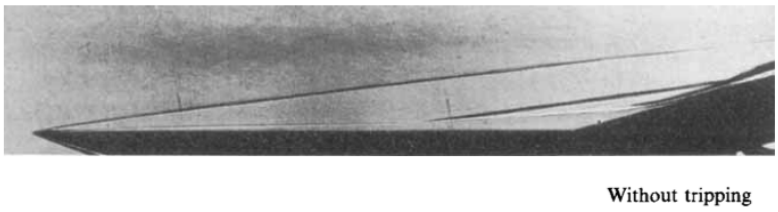

Figure 5: Schlieren photograph of test case 3 by Simeonides and Haase (1995).

4 Simulation Results and Discussion

4.1 Laminar

A laminar case was first run to serve as an initial condition for the three turbulent cases. The case was run to convergence and a restart file was created for the SST, SA, and BL cases.

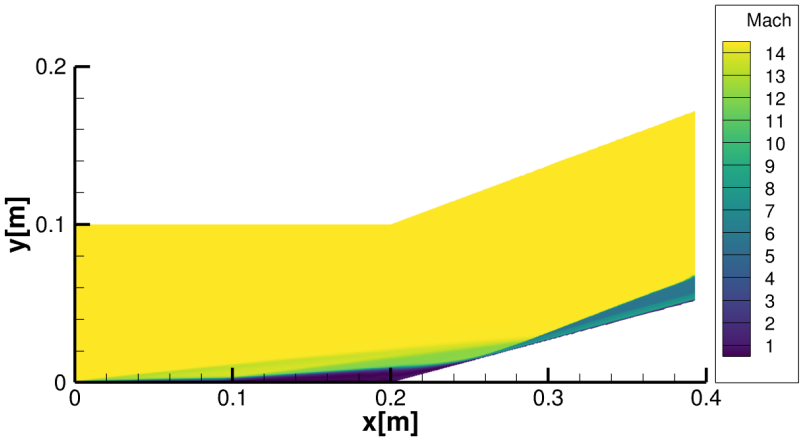

Figure 6: Mach contour for test case 3 for the laminar case

Seen in Figure 6 is a mach contour for the laminar case. A recirculation zone was observed to have formed above the corner and is constrained from the freestream ob an oblique shock. The boundary layer separates from the wall near $x = 0.1$ m and reattaches on the angled incline near $x = 0.25$ m. At the reattachment point, the oblique shock expected for an inviscid flow is formed at an angle of $\theta_s \approx 19°$.

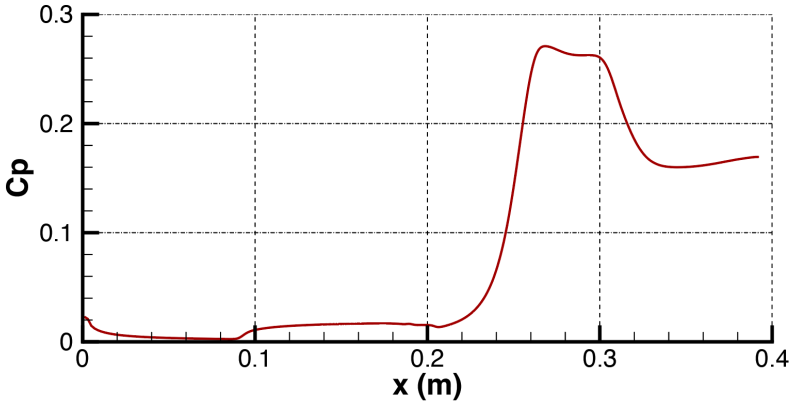

Figure 7: c_p along the wall for the laminar case.

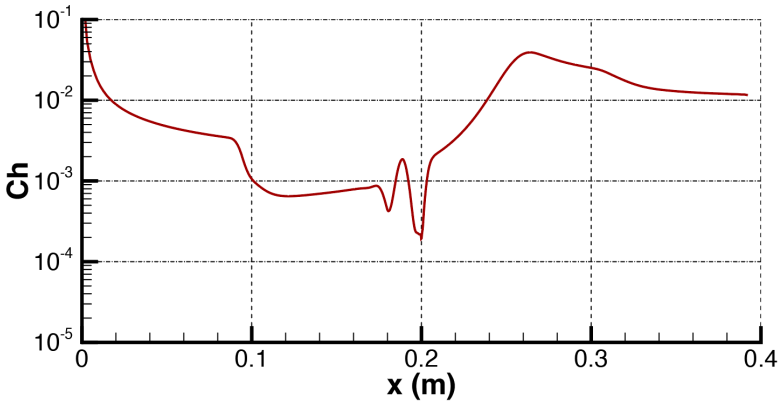

Figure 8: c_h along the wall for the laminar case.

Plots of c_p and c_h can be also be seen above. In comparing these results to Figures 3 and 5 it is clear that these results do not agree with the values observed by Simeonides and Haase (1995). Given more time, I would have preferred to investigate the reason for this discrepancy before moving on to turbulent cases. However key features from Simeonides and Haase (1995) are still present - notably the local peak in c_p near $x = 0.275$ m and the sharp decline in c_h near $x = 0.14$ m. For this reason the laminar case is still used as a comparison for the following turbulent cases.

4.2 Baldwin-Lomax

The BL model was first selected for investigation. Note that the Baldwin-Lomax model is a 0-equation algebraic model that cannot predict separation - thus it's success in modeling the recirculation zone was not expected. A contour plot of Mach number can be seen below in Figure 9. Note that the model was successful in maintaining a physical flow field. The recirculation zone and resultant oblique shock are still present.

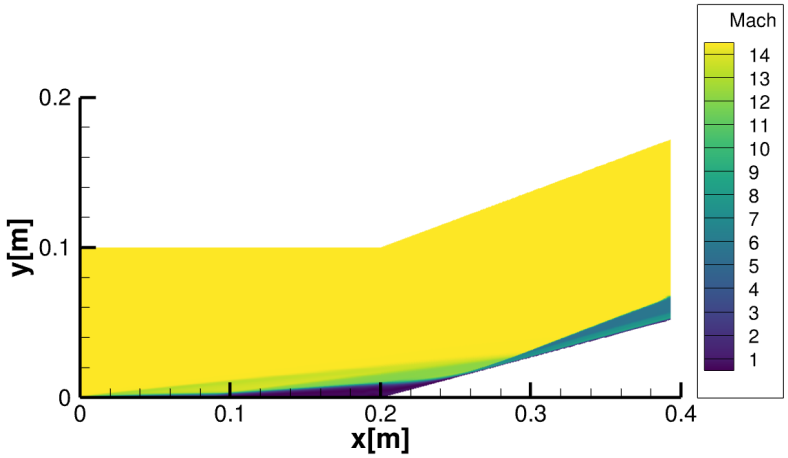

Figure 9: Mach contour for test case 3 using the Baldwin-Lomax turbulence model.

Seen below in Figures 10 and 11, we see *extremely* similar behavior compared to the previous laminar case. Specifically the peak in c_p is seen in the same location, as well as the sharp decline in c_h. Turbulent characteristics observed by Simeonides and Haase (1995) and discussed in section 3 are not found. From this, it is my conclusion that the BL turbulence model was unsuccessful in reproducing the expected results of this study. Though it's implementation and use with LeMANS was relatively simple, the fact that it cannot capture a broad range of flow physics, namely separation, makes it unsuitable for this study.

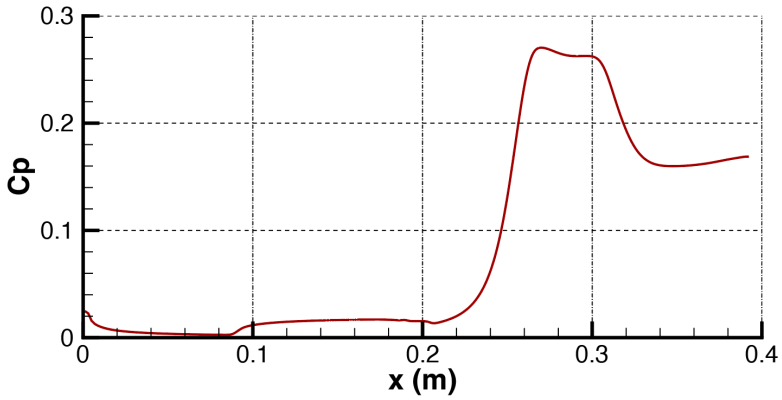

Figure 10: c_p along the wall for the Baldwin-Lomax case is seen to be very similar to the laminar case.

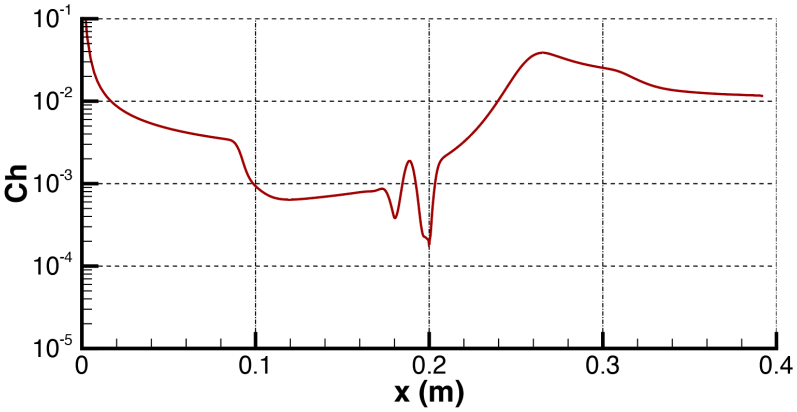

Figure 11: c_h along the wall for the Baldwin-Lomax case is seen to be very similar to the laminar case.

4.3 Spalart-Allmaras

The SA model is a one-equation turbulent viscosity model suited for aerodynamic/exterior flows. It has enjoyed great success in this area for its simplicity and it was my initial opinion that it would perform well for this case. A contour plot of Mach number can be seen below in Figure 12. Note that the SA model did not maintain the recirculation region.

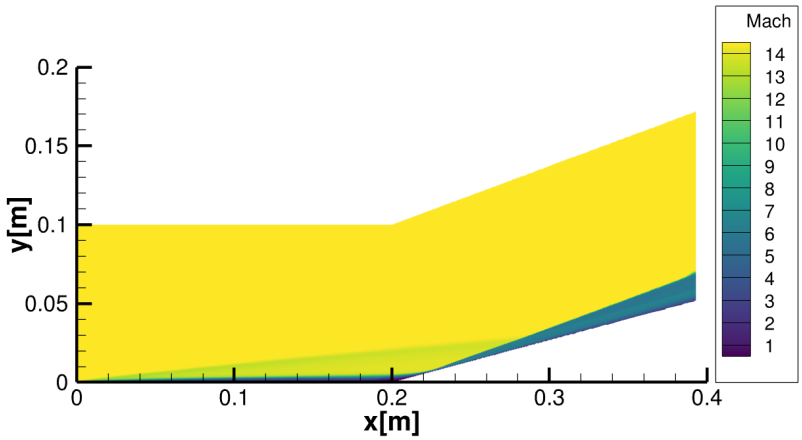

Figure 12: Mach contour for test case 3 using the Spalart-Allmaras turbulence model.

As the laminar case was used as an initial condition, it is clear that the SA model was responsible for the "destruction" of the recirculation region. Given more time, it would have been interesting to vary the turbulent freestream conditions an see if this behavior was the result of a poorly conditioned freestream.

Looking at the wall parameters in Figures 13 and 14, we see that the expected turbulent results were recovered. Specifically, c_p is seen to increase to a semi-constant value past the shock without a strong local maximum. Additionally, c_h is seen to smoothly decrease as it approaches the corner before increasing to a similar semi-constant value. This suggests that at least near the wall, the SA model is behaving as expected. However, there is still a large discrepancy in the magnitude of c_p and c_h compared to the results of Simeonides and Haase (1995) from Figures 3 and 5. As this is also present in the laminar case, it is my hypothesis that if the laminar case discrepancy was to be resolved this would logically follow through for the turbulent cases as well.

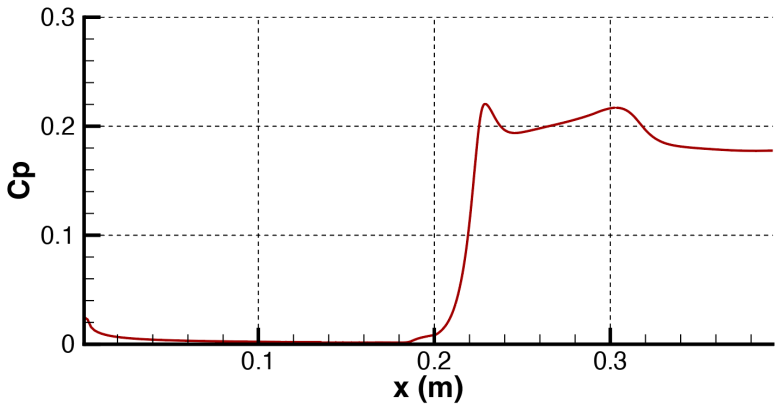

Figure 13: c_p along the wall for the Spalart-Allmaras turbulence model shows similar characteristics to Simeonides and Haase (1995).

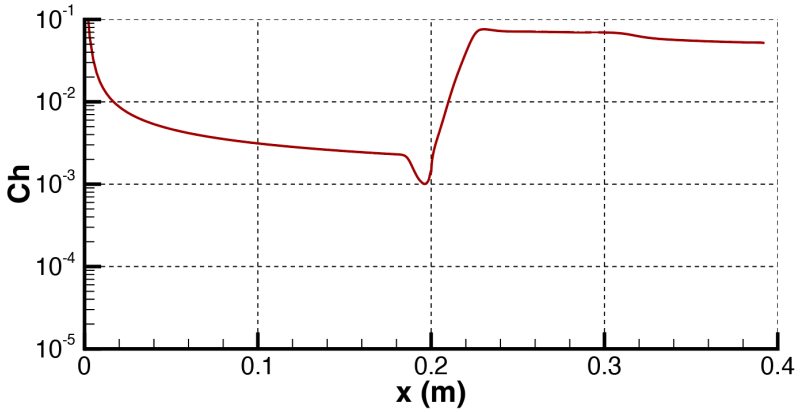

Figure 14: c_h along the wall for the Spalart-Allmaras turbulence model shows similar characteristics to Simeonides and Haase (1995).

4.4 Menter-SST

The SST model is a two-equation turbulent viscosity model that combines the best properties of the well known $k-\epsilon$ and $k-\omega$ models. Similarly to SA it has enjoyed much success and has sometimes been merited to be good for separating flow, thus, it was also my initial opinion that it would perform well for this case. A contour plot of Mach number can be seen below in Figure 15. Note that similarly to the SA model, the SST model did not maintain the recirculation region.

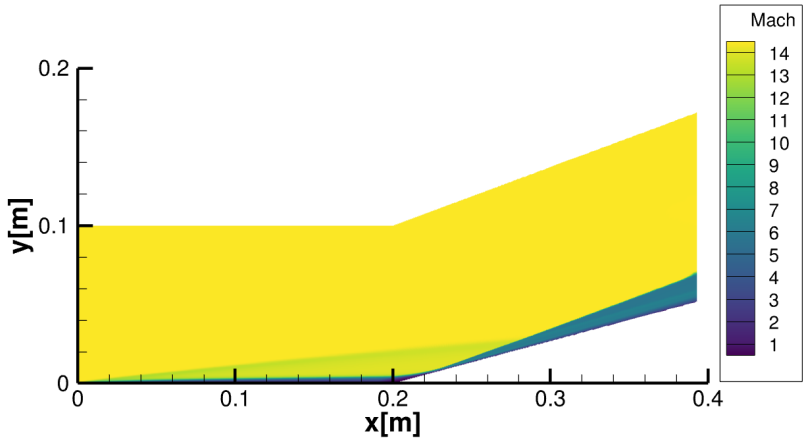

Figure 15: Mach contour for test case 3 using the Menter-SST turbulence model.

Clearly the SST model was responsible for the "destruction" of the recirculation region. It was brought to my attention that the boundary treatment of ω within the SST model may result in predicated behavior near the wall, as especially near the separated recirculation zone. This boundary treatment enforcing a value of ω at the wall is specified below where ν

is the kinematic viscosity and β_1 is a model constant.

$$\omega_{wall} = 10\frac{6\nu}{\beta_1(\Delta y)^2}$$

This treatment is necessary as the value of k approaches 0 at the wall, creating a singularity due to the definition of $\omega = \epsilon/k$. However, in the case of separation it is likely that a simple treatment of ω only at the wall is insufficient to capture desired flow qualities.

Viewing the wall parameters in Figures 16 and 17, we see that the expected turbulent results were recovered. As before, c_p is seen to increase to a semi-constant value and c_h is seen to smoothly decrease as it approaches the corner before increasing to a similar semi-constant value. In addition to the discrepancy of c_p and c_h compared to the results of Simeonides and Haase (1995), the SST model also predicts a much higher value of c_h past the corner compared to the SA model. The reason for this is unknown currently. Given more time, a grid convergence study would be the first place to start in order to ensure that the mesh has sufficient resolution for both models.

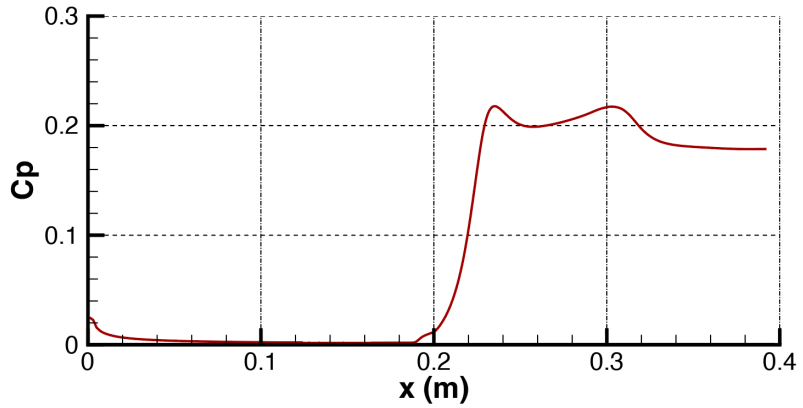

Figure 16: c_p along the wall for the Menter-SST turbulence model shows similar characteristics to Simeonides and Haase (1995).

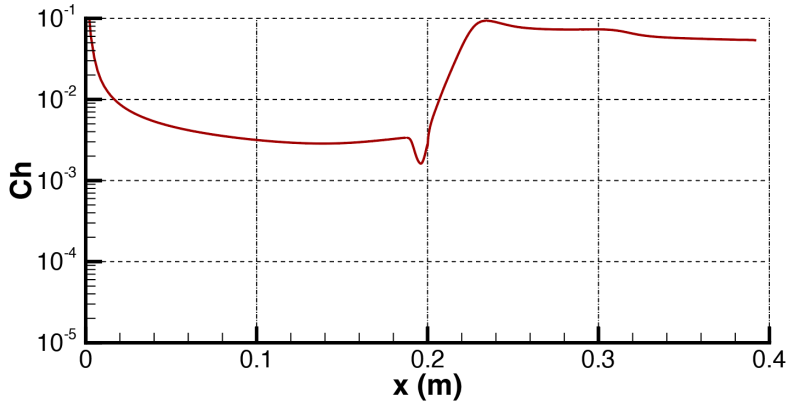

Figure 17: c_h along the wall for the Menter-SST turbulence model shows similar characteristics to Simeonides and Haase (1995).

5 Conclusions and Future Work

For this report three turbulence models were applied to the case of a hypersonic compression corner. These models were the 0-equation Baldwin-Lomax Model, the one-equation Spalart-Allmaras model, and the two-equation Menter-SST model. Flow fields were computed along with values of c_p and c_h along the wall and compared to experimental and computational data by Simeonides and Haase (1995). It was found that the BL model was unsuccessful in recreating turbulent behavior near the wall, but was successful in maintaining the experimentally observed recirculating zone. The SA and SST models were successful in recreating the general trends of c_p and c_h seen by Simeonides and Haase (1995), but did not maintain the recirculation region.

Given more time there are a few avenues I would wish to pursue to refine this project. Namely, I would first like to vary the turbulent boundary conditions near the freestream. Near the end of this project I realised that the experimental conditions of a shock tube likely have different freestream characteristics compared to the true in-flight condition as the flow is being accelerated by a normal shock. This could result in different behavior for the SA and SST models. Additionally, with the knowledge of the wall treatment of ω within the SST model, I would be interested in diving deeper into LeMANS to see if a modification to this treatment would allow it to fare better in a separated region. This would likely have to be more than just a simple enforcement at the wall in order to capture the behavior of a separated region, which may have complex flow far from the wall.

References

G. Simeonides and W. Haase, Journal of Fluid Mechanics **283**, 17–42 (1995).